Species separation of binary colloidal mixtures in the multi-Gauss potential: Effect of depletion*

Sun Zong-Li(孙宗利)[a)†], Kang Yan-Shuang(康艳霜)[b)], Kang Yan-Mei(康艳梅)[c)], and Song Jian-Min(宋建民)[b)]

[a)] *Science and Technology College, North China Electric Power University, Baoding* 071051, *China*
[b)] *College of Science, Agriculture University of Hebei, Baoding* 071001, *China*
[c)] *University of International Relations, Beijing* 100091, *China*

(Received 8 June 2014; revised manuscript received 22 June 2014; published online 10 October 2014)

For the asymmetrical colloidal mixture subject to a confining potential and an external multi-Gauss potential, the separation of species is studied based on the classical density functional theory of simple fluids. The multi-Gauss potential consists of several Gauss barriers, which are distributed along the axial direction with uniform distance. The barrier width, barrier distance, and barrier height are individually adjusted to investigate their effects on the species separation. From the numerical results, it is concluded that in each condition, the competition between the external potential and the depletion potential determines the phase equilibrium and the separation. Species separation appears only in the region where the depletion is dominant. On the contrary, both species are absent in the regions where the external potential takes the absolute advantage.

Keywords: depletion, demixing, colloidal mixture, density functional theory

PACS: 64.75.Xc, 61.20.Gy **DOI:** 10.1088/1674-1056/23/12/126401

1. Introduction

The process of demixing in colloidal suspensions is determined by the depletion interaction, which is proposed by Asakura and Oosawa (AO),[1] and later, individually by Vrij.[2] In the asymmetric mixtures, the big particles exclude the small ones from existing in the gap between them. Anisotropy of the local osmotic pressure leads to the attraction between the big particles. In fact, the range and strength of the attractive potential are mainly determined by the size ratio between the asymmetric species. From this point of view, the depletion interaction is entropically driven in nature. Theoretically, the depletion interaction describes well the structural features and phenomena in colloidal systems including the biological ion channels[3–6] and the colloid-polymer mixtures.[7–12] Besides, for the systems in which the bare inter-particle force is purely repulsive, it can provide satisfactory interpretation about the microscopic mechanism of their static and dynamical processes.

Prioring to the determination of depletion potential and its effect on the structure of colloidal suspensions, the system should be firstly modeled. As in the simple AO model, the colloid–colloid interaction is usually treated as additive hard-sphere potential. Actually, using layers of poly-12-hydroxystearic acid (PHSA) adsorbed onto mica sheets in a surfaces force apparatus, Bryant *et al.*[13] had found that the adsorbed layers have no long-range attraction. In any experimental condition, the equation of state from their experimental results coincides with that of perfect hard-sphere system with the same volume fraction. Additionally, besides the additive hard sphere potential in the AO model, attractive Yukawa[14] and attractive multi-Yukawa[15] potential are the effective alternatives in the modeling of the colloidal particles and their mixtures. In Ref. [16], based on the two Yukawa potential models, Yu *et al.* studied the effect of the depletion interaction on the thermodynamic and structural properties. The satisfactory agreement between their analytical results and the simulation results suggests that the two Yukawa potentials possess the convincing ability to capture crucial features of colloidal mixtures.

Owing to its importance in colloidal suspension, much attention had been paid to the depletion interaction and its effect on the structure transition and phase equilibrium.[7–12,17,18] However, most of these reports focused on the hard potential or a soft potential but with a hard core, such as two big hard spheres in a reservoir of small hard sphere, or one big hard sphere and a fixed object immersed in a sea of small particles.[17,18] The hard potential between the big particles, or between the big sphere and the fixed object excludes all the small particles in their crossed depletion regions. Actually, the external potential with finite strength, which can be penetrated or tunnelled, can also invokes depletion so that the big particles can be pushed towards the center of the barrier. On the contrary to the conditions of hard potential, finite external potential cannot excludes all the particles within its scope. Even so, effective attraction still emerges due to the difference in the local osmotic pressure. Few works relating to such a phenomenon has been reported very recently. By using the equi-

*Project supported by the Fundamental Research Funds for the Central Universities, China (Grant No. 13MS105).
†Corresponding author. E-mail: zongli_sun@163.com
© 2014 Chinese Physical Society and IOP Publishing Ltd

librium density functional theory (DFT) and dynamical DFT, Roth *et al.*[19] studied the size selectivity in binary colloidal mixture, which is confined by the applied repulsive or attractive external potentials. Potential dependence of selectivity is observed near the center of the external potential. Kumar[20] performed the Monte Carlo simulations in the canonical ensemble to study the effect of depletion on the demixing in the binary colloidal mixtures, which are confined in a quasi-one dimensional simulation box. Their calculation and analysis about the demixing suggested that overlap of depletion layers of the big particles and that of repulsive potential enhances the demixing.

Prompted by the works mentioned above, we construct in this work a finite external potential with more complex geometry, the multi-Gauss potential. Adjustment of its geometry causes the change in the depletion for the big particles, because the depletion due to each Gauss barrier may couple with each other. For the system subject to such an external potential, its equilibrium structure may be conveniently modulated. Experimentally, the external potential can be realized utilizing the laser beams. Accordingly, the geometry of the multi-Gauss potential can be adjusted through the modulation of the characteristics and intensity of the laser beams. Therefore, this work aims to investigate the effect of depletion on the equilibrium structure of the binary colloidal mixture, as the geometry of the external potential is adjusted.

Theoretically, depletion in binary hard-sphere colloidal mixtures has been investigated by various theoretical tools including thermodynamical perturbations theory (TPT),[21,22] DFT,[23–25] and integral equations theory (IET).[26–29] Among these treatments, DFT[30–32] is the most powerful and popular one because its satisfactory performance has been obtained for the systems rangeing from simple Lennard-Jones fluids[33,34] to the colloidal particles.[17,18] Despite the lack of knowledge about the exact expression for the excess Helmholtz free energy or the first-order direct correlation function (DCF) for the practical system, the density functional approximations (DFA), including functional perturbation expansion approximation (FPEA),[35–37] bridge density functional approximation (BDFA),[38–40] weight density approximation (WDA),[41,42] and fundamental measure theory (FMT),[43] have been developed in the application of DFT to the simple fluids. In this paper, the modified version of fundamental measure theory (MFMT)[44,45] is employed to express the excess Helmholtz free energy contributed from the colloid–colloid interaction.

The paper is organized as follows. In Section 2, the system under consideration is modeled and described. The frameworks of DFT and MFMT are also concisely reviewed in Section 2. In Section 3, to check the codes used in this work, our results for the system with single Gauss barrier are compared with those from Monte Carlo simulation. Further, the effects of the barrier width, barrier distance, barrier height, and size ratio on the phase separation are calculated and analyzed. A short summary is presented in Section 4.

2. Model and theory

2.1. Modeling of the confined binary colloidal mixture

In this paper, the system under consideration consists of a binary colloidal mixture, which is composed by small and big colloidal particles with diameters $\sigma_{\rm s}$ and $\sigma_{\rm b}$. For simplicity, the additive hard-sphere potential is employed to model the intra- and inter-species interactions. That is, $\sigma_{\rm bs} = (\sigma_{\rm bb}+\sigma_{\rm ss})/2$. This system is confined symmetrically in a one-dimensional box, whose boundaries locate at $z=0$ and $z=H$. The potentials felt by the species are:

$$V_{{\rm conf},\nu}(z) = \varepsilon_{\rm conf}\left(\frac{z-z_0}{L_\nu}\right)^m, \tag{1}$$

with ν = b, s distinguishing the species in the mixture. $\varepsilon_{\rm conf}$ is the strength of the confining potential. $m=20$ is set in this work so that the confining potential in Eq. (1) can be regarded as that produced by a slightly soft slit pore with a width $h=2L$. It is easy to find that $H=2z_0$ with z_0 the midpoint of the box. $L_\nu \equiv L+\sigma_\nu/2$ with L denoting the half separation of the parallel confining walls.

Besides, the mixture is subject to an external potential $V_{\rm ext}(z)$, which is composed of n Gauss barriers:

$$V_{\rm ext}(z) = \sum_{i=1}^{n}\varepsilon_i \exp\left[-\left(\frac{z-z_i}{w_i}\right)^2\right], \tag{2}$$

where ε_i and z_i are respectively the strength and position of the i-th Gauss barrier. The parameter w_i characters the width of Gauss barriers. Note that the external potential $V_{\rm ext}(z)$ can be experimentally realized by n individual Gaussian laser beams, to which the colloidal particles can sensitively respond. Moreover, the geometry of $V_{\rm ext}(z)$ can also be conveniently changed by the modulation of the laser beams. Accordingly, the total potential $V_\nu(z)$ felt by the species is the sum of the two, that is, $V_\nu(z) = V_{{\rm conf},\nu}(z) + V_{\rm ext}(z)$. In the equilibrium of the system, the applied external potential is the most important factor determining the inhomogeneity of density. The character of $V_{\rm ext}(z)$ influences directly the pattern of density profile, which will in turn determine the depletion. Particularly, changes in the barrier width, barrier distance, and barrier height will modulate the depletion, and therefore the species separation in the trap.

2.2. DFT for the binary hard-sphere mixture

According to the classical DFT,[30–32] the grand potential functional $\Omega[\rho_\nu(\boldsymbol{r})]$ for mixtures is formally expressed as:

$$\Omega[\rho_\nu(\boldsymbol{r})] = \mathscr{F}[\rho_\nu(\boldsymbol{r})] + \sum_\nu \int \rho_\nu(\boldsymbol{r})[V_\nu(\boldsymbol{r})-\mu_\nu]\,{\rm d}\boldsymbol{r}, \tag{3}$$

where μ_ν is chemical potential of a particle in bulk phase of the ν-th species and $\mathscr{F}[\rho_\nu(\boldsymbol{r})]$ is the corresponding intrinsic Helmholtz free energy. As is well known, $\Omega[\rho_\nu(\boldsymbol{r})]$ is minimized when the system is in equilibrium, and the equilibrium density profile $\rho_\nu(\boldsymbol{r})$ satisfies the variation principle:

$$\frac{\delta\Omega[\rho_\nu(\boldsymbol{r})]}{\delta\rho_\nu(\boldsymbol{r})} = 0. \tag{4}$$

For hard sphere fluids, $\mathscr{F}[\rho_\nu(\boldsymbol{r})]$ can be perturbatively split into contributions from ideal gas and hard sphere repulsion. That is:

$$\mathscr{F}[\rho_\nu(\boldsymbol{r})] = \mathscr{F}_{\rm id}[\rho_\nu(\boldsymbol{r})] + \mathscr{F}_{\rm hs}[\rho_\nu(\boldsymbol{r})]. \tag{5}$$

Expression for $\mathscr{F}_{\rm id}$ is exactly known as $\mathscr{F}_{\rm id} = k_{\rm B}T\sum_\nu \int \rho_\nu(\boldsymbol{r})[\ln(\lambda_\nu^3\rho_\nu(\boldsymbol{r})) - 1]\,{\rm d}\boldsymbol{r}$ with λ_ν denoting the thermal wavelength. $k_{\rm B}$ and T are respectively the Boltzmann constant and absolute temperature. However, exact expression for $\mathscr{F}_{\rm hs}$ is unknown for most practical systems. Therefore, approximation for it is necessary to implement the calculations. Among all the DFAs, MFMT[44,45] for hard sphere fluids has shown more satisfactory performance in predicting the structure, phenomena transitions, and thermodynamic properties of inhomogeneous fluids. Thence, in this work, MFMT is employed to express $\mathscr{F}_{\rm hs}[\rho_\nu(\boldsymbol{r})]$.

According to the MFMT for mixtures,[46] $\mathscr{F}_{\rm hs}$ is given by:

$$\begin{aligned}&\beta\mathscr{F}_{\rm hs}\\ &= \int\Bigg\{-n_0\ln(1-n_3) + \frac{n_1n_2 - \boldsymbol{n}_{\rm I}\boldsymbol{n}_{\rm II}}{1-n_3}\\ &\quad + \frac{1}{36\pi}\left[n_3\ln(1-n_3) + \frac{n_3^2}{(1-n_3)^2}\right]\frac{n_2^3 - 3n_2\boldsymbol{n}_{\rm II}^2}{n_3^3}\Bigg\}{\rm d}\boldsymbol{r},\end{aligned} \tag{6}$$

where $\beta = 1/k_{\rm B}T$ and $n_\alpha(\boldsymbol{r}) = \sum_\nu \int \rho_\nu(\boldsymbol{r}')\omega_\nu^{(\alpha)}(\boldsymbol{r}-\boldsymbol{r}')\,{\rm d}\boldsymbol{r}'$ ($\alpha = 0,1,2,3,{\rm I},{\rm II}$) is the weighted densities, with $\omega_\nu^{(\alpha)}$ denoting the density-independent weight functions, whose explicit form can be found in Refs. [44]–[47].

Given the particle number N_ν and the external potential, the equilibrium density profiles $\rho_\nu(\boldsymbol{r})$ can be numerically solved by minimizing the grand potential functional under the constraint $\int \rho_\nu(\boldsymbol{r})\,{\rm d}\boldsymbol{r} = N_\nu$. This leads to the following coupled integral equations:

$$\rho_\nu(\boldsymbol{r}) = N_\nu\frac{\exp[-\beta(V_\nu(\boldsymbol{r})) + c^{(1)}(\boldsymbol{r};\rho_\nu)]}{\int\exp[-\beta(V_\nu(\boldsymbol{r})) + c^{(1)}(\boldsymbol{r};\rho_\nu)]\,{\rm d}\boldsymbol{r}}, \tag{7}$$

which can be solved by using the Picard-type iterative method. In Eq. (7),

$$c^{(1)}(\boldsymbol{r};\rho_\nu) = -\beta\frac{\delta\mathscr{F}_{\rm hs}[\rho_\nu(\boldsymbol{r})]}{\delta\rho_\nu(\boldsymbol{r})}$$

is the first order DCF of the ν-th species. Noting that in this paper, we control the particle number N_ν by adjusting the volume fraction of each species, which is defined as $\eta_\nu = \pi\sigma_\nu^3\rho_\nu^b/6$ with $\rho_\nu^b = N_\nu/H$.

3. Results and discussion

Theoretically, it is worthy noting that the multi-Gauss potential defined in Eq. (2) creates depletion regions, where the smaller particles are partially excluded. The equilibrium structure of the mixture is determined by the competition between the external potential and the depletion potential induced by it. This is the manner in which the external potential influence the equilibrium of the mixture.

Employing the MFMT in the computation of the DCFs, the equilibrium density of each species can be calculated within the framework of DFT. To valuate the performance of our codes for the calculation, the density profiles of both species are compared in Fig. 1 to those from the Monte Carlo simulation[20] in the case of single Gauss barrier, which locates at the midpoint, say z_0, of the pore. In our calculation, we choose $\varepsilon_{\rm conf}/k_{\rm B}T = 10.0$, $\varepsilon_1/k_{\rm B}T = 2.0$, $z_0/\sigma_{\rm s} = 10.24$, $L/\sigma_{\rm s} = 7.5$, $\sigma_{\rm b}/\sigma_{\rm s} = 2.0$ as in the simulation performed by Kumar.[20] In Figs. 1(a), 1(b), and 1(c), the total volume fraction $\eta_{\rm tot} = \eta_{\rm s} + \eta_{\rm b}$ are respectively set as 0.1, 0.2, 0.3. The two species have the equal volume fraction, that is $\eta_{\rm s} = \eta_{\rm b}$.

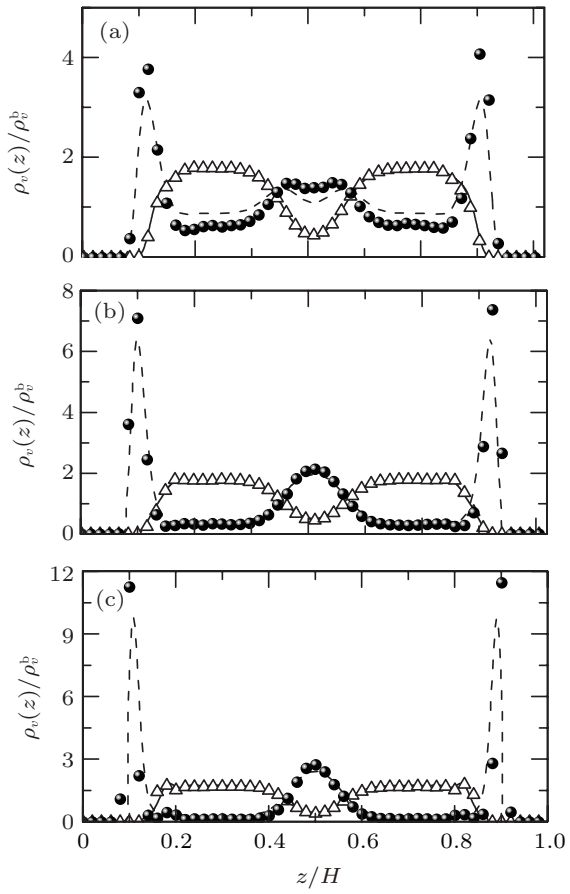


Fig. 1. Equilibrium density profiles of the binary mixture along the z direction under the conditions of $\varepsilon_{\rm conf}/k_{\rm B}T = 10.0$, $\varepsilon_i/k_{\rm B}T = 2.0$, $z_0/\sigma_{\rm s} = 10.24$, $L/\sigma_{\rm s} = 7.5$, and $\sigma_{\rm b}/\sigma_{\rm s} = 2.0$. The width of the barrier is set as $w/\sigma_{\rm s} = 1.5$ in the calculations. (a) For $\eta_{\rm tot} = 0.1$, (b) for $\eta_{\rm tot} = 0.2$, and (c) for $\eta_{\rm tot} = 0.3$. The solid and dash lines correspond respectively to the small and big species, while the symbols correspond to the simulation results in Ref. [20].

Comparison in Fig. 1 shows that our results agree generally well with those from the simulation. Besides, one can see that for the case of $\eta_{\rm tot} = 0.1$, the density of big species is underestimated near the depletion layer, which arises from the single Gauss barrier at z_0. As the total volume fraction is increased, the deviation is suppressed. Moreover, from Figs. 1(a)–1(c), one can see that our results deviate always from those from simulation in the regions near the wall. Actually, the pair interaction employed in our model is different from that used in the simulation, which takes into account the long ranged repulsive tail. The difference in the pair interaction is responsible for the deviation near the walls.

Generally speaking, the depletion interaction in the binary mixture is influenced by a number of factors, among which the geometry of the external potential is most important because of its convenient realization in experiments. In the following calculations, we take n =7, which means that the external potential is designed with seven Gauss barriers, whose position and height can be modulated individually to control its geometry. Noting that the external potential keeps symmetrical about the midpoint z_0, at which locates one Gauss barrier. The other barriers distribute along the z axial direction with a uniform distance of $\xi \equiv z_{i+1} - z_i$. As an indispensable ingredient in the grand potential functional, the external potential determines directly the equilibrium structure. Besides, the local density of each component will influence the depletion potential, which in turn leads to modulation of the structures in the mixture. In the following, the DFT is used to investigate the influence of the geometry of the external potential on the species separation.

3.1. Effect of barrier width on the species separation

Firstly, the effect of barrier width on the species separation is investigated. Barrier width determines the region where the depletion appears. Accordingly, different structures may emerge when the barrier width is adjusted. In Fig. 2(a), the curves for the external potentials with different barrier widths are plotted. From these curves, one can see that the barriers couple with each other when their width is large enough. The coupling between barriers will ultimately influence the density of both species. In addition, as an important ingredient of the total potential, the confining potential $V_{{\rm conf},v}(z)$ may also influence the external potential $V_{\rm ext}(z)$. Due to the short-ranged nature of the confining potential, the interplay between the two ingredients is significant only in the region near the walls. The barriers in the middle region of the pore keep their Gaussian nature. This is clearly shown in Fig. 2(b). Note that the two Gauss barriers on both ends of the pore are unobservable in the curves because of their coupling with the strong confining potential. Similar manner of the total potentials can also be shown for the curves in Figs. 5 and 7 below, while it is not plotted for concise.

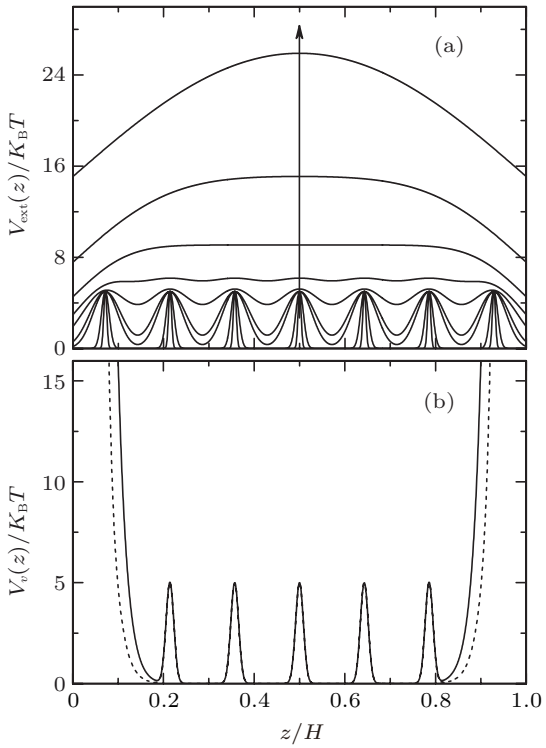


Fig. 2. (a) Profiles of the external potential $V_{\rm ext}(z)$ along the z direction in different conditions of barrier width. Along the arrow, the barrier widths are respectively $w_i/\sigma_{\rm s} = 0.1$, 0.25, 0.8, 1.0, 1.5, 2.0, 3.0, 5.0, 10.0. (b) Profiles of the total potential $V_v(z)$ along the z direction under conditions of $w_i/\sigma_{\rm s} = 0.25$ and $\xi/z_0 = 2/7$. The solid and dash lines in panel (b) correspond respectively to the potentials felt by the small and big particles.

In Fig. 3, we have calculated the effect of the barrier width w_i on the equilibrium structure. In the calculation, we have set $\varepsilon_{\rm conf}/k_{\rm B}T = 10.0$, $z_0/\sigma_{\rm s} = 10.24$, and $L/\sigma_{\rm s} = 7.5$ for the confining potential, while for the multi-Gauss potential, we choose for all the seven Gauss barriers $\varepsilon_i/k_{\rm B}T = 5.0$ and $\xi/z_0 = 2/7$. The volume fraction and size asymmetry are respectively $\eta_{\rm s} = \eta_{\rm b} = 0.1$ and $\sigma_{\rm b}/\sigma_{\rm s} = 2.0$. From Figs. 3(a)–3(i), the barrier width are set respectively as $w_i/\sigma_{\rm s} = 0.1, 0.25, 0.8, 1.0, 1.5, 2.0, 3.0, 5.0, 10.0$.

From the results in Fig. 3, one can see that the species separation are modulated obviously by the barrier widths. When the barriers are narrower, species separation with spatial periodicity is observed in most region of the pore, such as in Figs. 3(a)–3(e). With the increase of w_i, the periodic oscillation structure of each species in the middle region disappears. However, further increase of w_i leads again to obvious species separation in the middle region.

This can be understood as follows. For the narrower barriers, the distance between them is so large that there is no coupling between them. In this condition, the depletion layer around each barrier does not overlap, which indicates that each barrier serves as a single barrier. In addition, the occurrence of the spatial periodicity is due to the uniform distribution of the

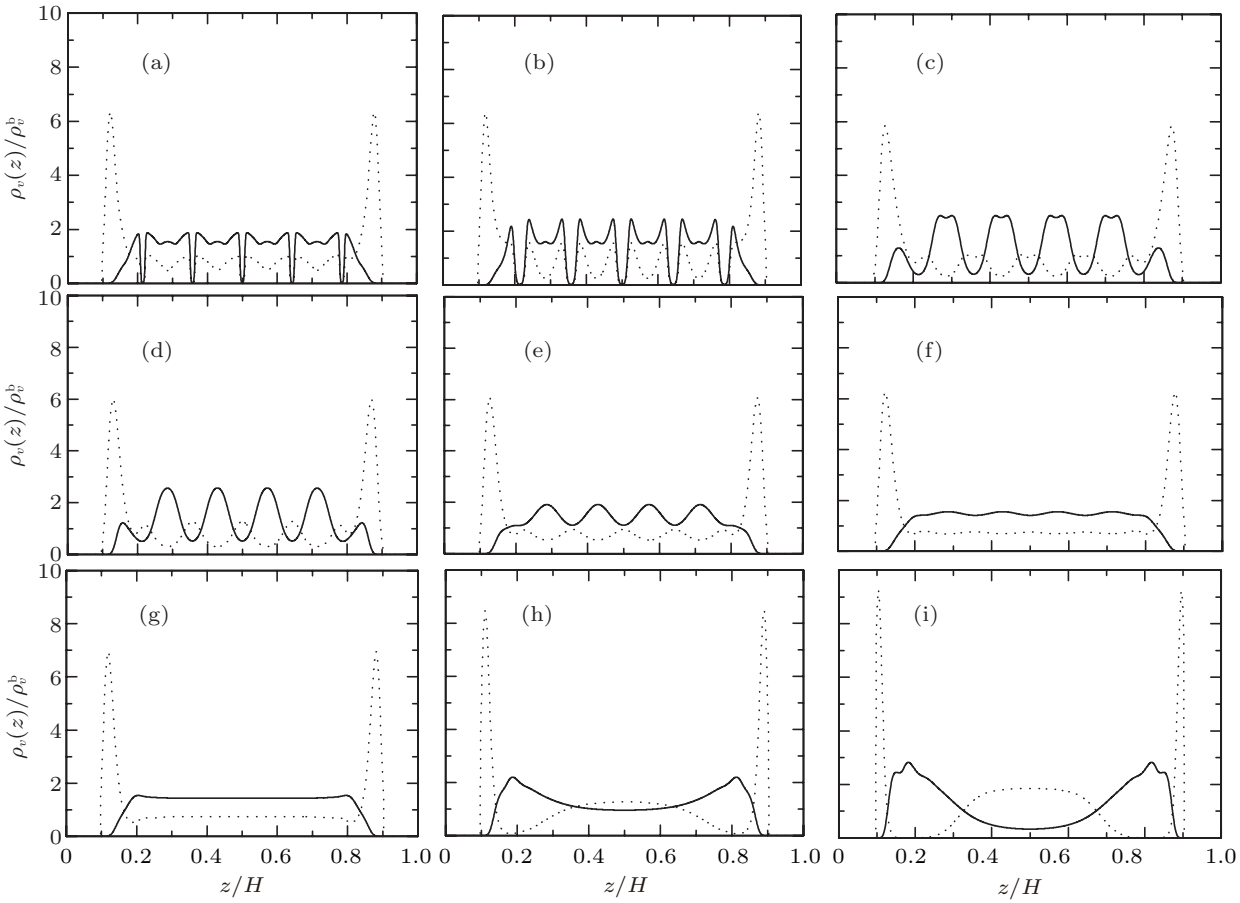


Fig. 3. Equilibrium density profiles of the binary mixture along the z direction under different conditions of barrier width. Panels (a)–(i) correspond respectively to $w_i/\sigma_s = 0.1, 0.25, 0.8, 1.0, 1.5, 2.0, 3.0, 5.0, 10.0$. The solid and dash lines correspond respectively to the small and big species.

barriers. On the contrary, for the barriers with moderate width, their uniform distribution leads to a nearly uniform profile of potential in the middle region, which suppresses the formation of the depletion layers. With further increase of w_i, each of barriers is so wide that it can couple with nearly all the other ones. This results in such a condition that the depletion layer of the barrier coincides with each other, which corresponds to the condition of single Gauss barrier, just as shown in Fig. 2.

Another interesting phenomenon shown in Figs. 3(a) and 3(b) is that at the center of each barrier, densities for both species show a minimum and no species separation is observed. This is the result of the competition between the external potential and the depletion potential. When the barriers are extremely narrow and sharp, the spatial gradient of external potential is very large, which leads to a large external force in these regions. Such a strong external force expels both species away from the center of the barriers.

To understand the physics in the above process, the chemical potentials of both species are calculated. The results shown in Fig. 4 suggest that with the increase of w_i, the chemical potentials of both species are increased. This can be explained by making use of the definition of chemical potential, which measures the energy required to insert one more particle into the system. When the width of barriers is small, the inserted particle is mainly influenced by the barrier near its position. The barriers locating far away from the inserted particle contribute little because of their finite width. However, when the barriers are wider, the inserted particle may feel interaction from more than one barrier. Accordingly, more energy is required to insert the new particle, which corresponds to a larger chemical potential.

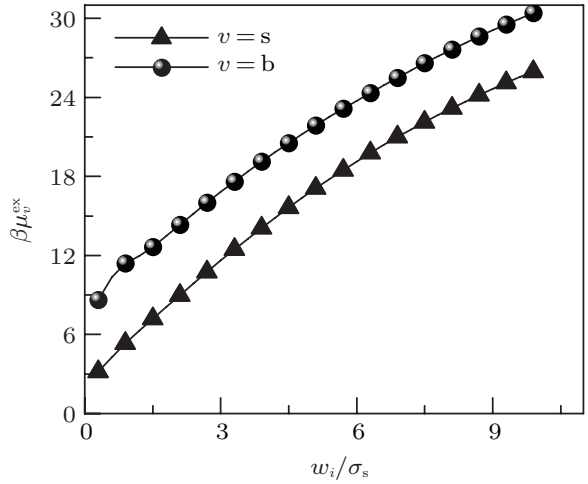


Fig. 4. Effect of barrier width on the chemical potential of both species. In the calculation, we choose $\varepsilon_i/k_BT = 5.0$, $\xi/z_0 = 2/7$, $\eta_s = \eta_b = 0.1$, and $\sigma_b/\sigma_s = 2.0$.

3.2. Effect of barrier distance on the species separation

From the results in Fig. 3, it has been seen that adjusting the barrier width leads to the coupling between the barriers, which causes the change in the phase equilibrium. Besides, the coupling between barriers can also arise from the adjustment in the barrier distance, which may cause a different influence on the external potential and further on the equilibrium structure. The curves for the external potential have been plotted in Fig. 5, which shows clearly the coupling of the barriers when the barrier distance is adjusted. The distribution of these barriers keeps equidistant and symmetrical about the midpoint z_0. Noting that when the barrier distance is small enough, the external potential tends to a new Gauss barrier, but with a larger height.

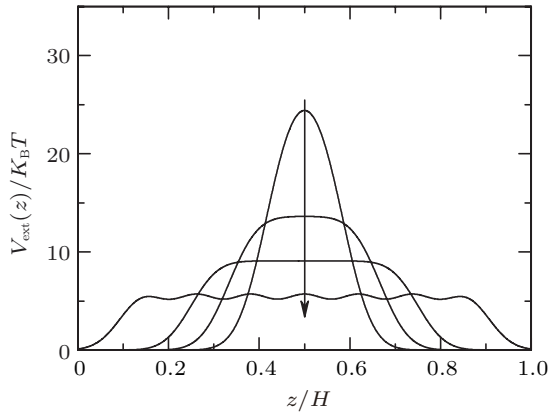


Fig. 5. Profiles of the external potential $V_{ext}(z)$ along the z direction under different conditions of barrier distance. Along the arrow, the barrier distance are respectively $\xi/z_0 = 1/21$, 2/21, 3/21, 5/21.

The density profiles for both species in different cases of barrier distance are plotted in Fig. 6. It is obvious that when the barrier distance is large, the curve for smaller species shows periodic oscillations in the region where the external potential can reach, while the larger species is nearly uniform there, as shown in Fig. 6(a). This indicates that the coupling between barriers is weak and the density of each species is mainly determined by the individual barrier in the local region.

With the decrease of the barrier distance, however, the structure of both species can be modulated significantly. On one hand, the smaller particles are expelled out from the central region by the stronger external potential. This causes immediately the congregation of smaller particles in the region next to the central region. Such a process enhances simultaneously the depletion interaction of the big particles, which leads directly to the increase of density of big particles in the central region. On the other hand, with further increase of barrier distance, the equilibrium structure is determined by the competition between the depletion and the external potential. Enhanced external potential in the central region expels both small and big particles. When the external potential dominates the competition, the big particles are also expelled out. This suppresses the species separation in the central region, as shown in Fig. 6(c). Moreover, when the external potential in the central region is strong enough, neither species is found there. In this condition, the external potential serves as a wall, which depletes all the particles and leads to depletion layers on its both sides, just as indicated in Fig. 6(d).

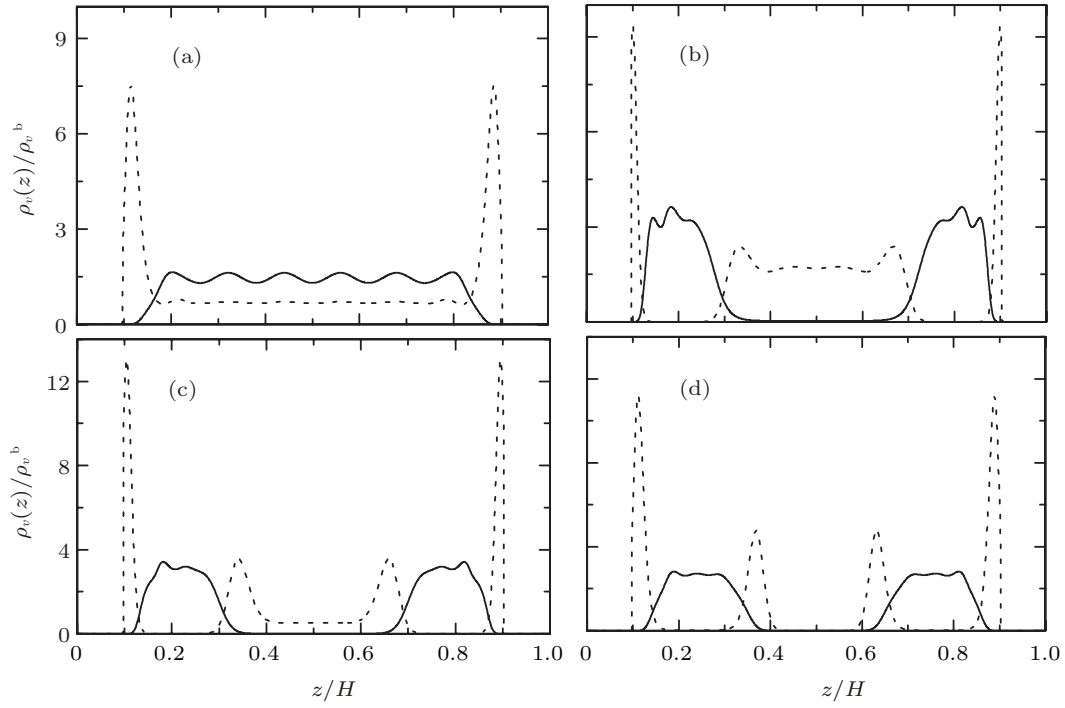


Fig. 6. Equilibrium density profiles of the binary mixture along the z direction under different conditions of barrier distance. Panels (a)–(d) correspond respectively to $\xi/z_0 = 1/21$, 2/21, 3/21, 5/21. The solid and dash lines correspond respectively to the small and big species.

3.3. Effect of barrier height on the species separation

To get a comprehensive understanding about the effect of the geometry of external potential on the species separation, we turn our attention to the barrier height in the following. As shown in Fig. 7, it is assumed that only the two barriers locating close to z_0 can be adjusted in height, for the purpose that the density profiles can show distinctive difference in the local regions where barriers with different height locates. Theoretically, change in external potential may lead directly to the change in density for both species. Besides, the strength of depletion interaction between the barriers and the big particles also relates to the barrier height. The larger the height of the barriers, the stronger the depletion is there. These two effects compete with each other because they cause the opposite influence on the density of species.

The density profiles for both species in different cases of barrier height are calculated in Fig. 8. Comparison between the results suggests that with the adjustment of barrier height, the obvious change in density profile appears in three regions. One is the central region near the midpoint z_0, the other two are in the regions where locate the adjustable barriers. When the height of the adjustable barrier is small, the density of big particle is smaller than that of small particle in the region where locates the adjustable barriers, as shown in Fig. 8(a). This is the result of the depletion interaction. The effective attraction between big particles leads to their congregation towards to the barrier at z_0.

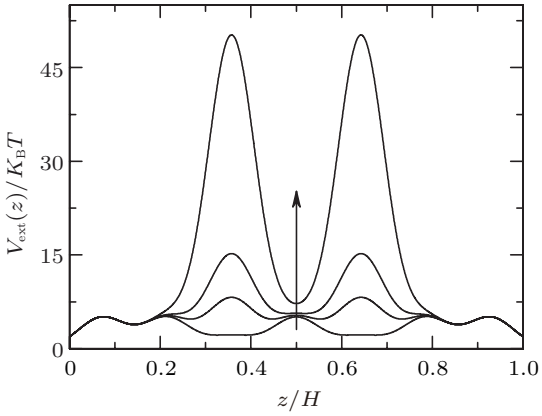


Fig. 7. Profiles of the external potential $V_{\rm ext}(z)$ along the z direction under different conditions of adjustable barrier height. Along the arrow, the adjustable barrier heights are respectively set as $\varepsilon/k_{\rm B}T = 2.0, 8.0, 15.0, 50.0$.

As the heights of the two barriers are slightly larger than that of the barrier locating at z_0, the central region is rich in small particles and large particles congregate near the two higher barriers, as shown in Fig. 8(b). This indicates that the depletion near the central barrier decreases while the depletion near the two higher barriers increases. Results in Fig. 8(c) show that further increase of the height will lead to the reduction of big particle in the region near the two higher barriers because of the competition between the external potential and the depletion potential there. When their height is large enough, the external potential is dominate and both big and small particles are expelled out from these regions, as shown in Fig. 8(d).

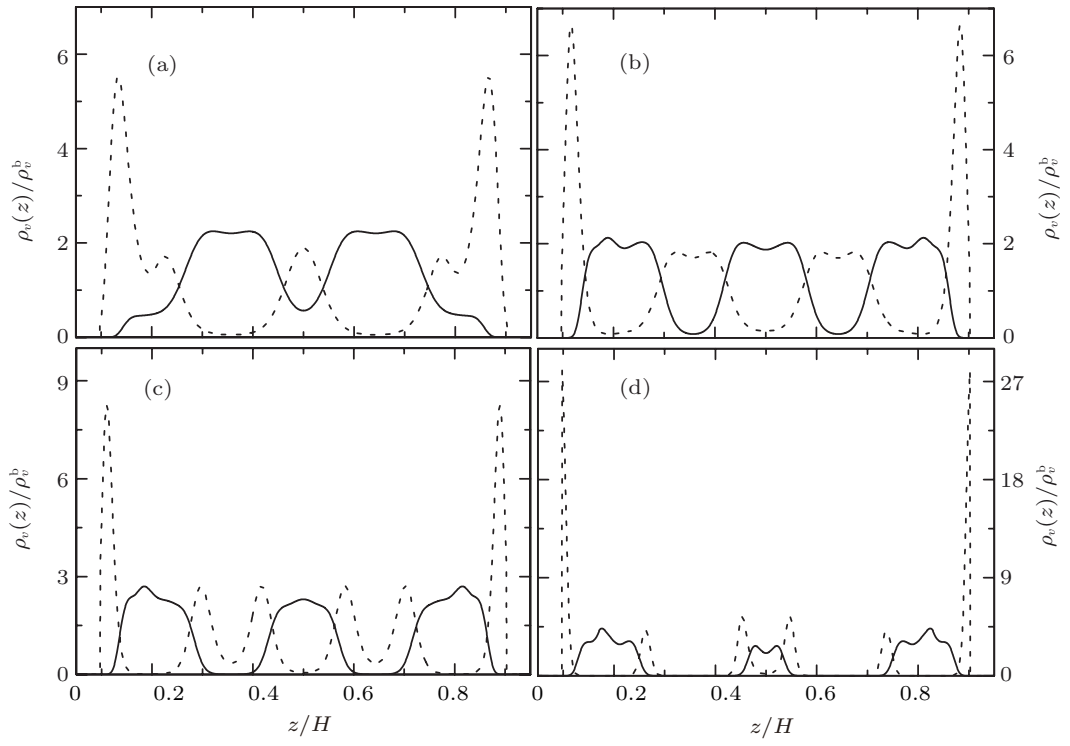


Fig. 8. Equilibrium density profiles of the binary mixture along the z direction under different conditions of adjustable barrier height. Panels (a)–(d) correspond respectively to $\varepsilon/k_{\rm B}T = 2.0, 8.0, 15.0, 50.0$. The solid and dash lines correspond respectively to the small and big species.

3.4. Effect of size ratio between the species

In the above calculations, it is suggested that the depletion interaction is responsible for the species separation when the mixture is exposed to an external potential, and that the competition between the depletion and the external potential determines the equilibrium configurational structure of the mixture. However, for the given external potential, the mixtures with different size ratios may show different structural properties due to the different strengths of the depletion.

The density profiles for both species in different cases of size ratios are calculated in Fig. 9. In the calculations, $\varepsilon_{\rm conf}/k_{\rm B}T = 10.0$, $\varepsilon_i/k_{\rm B}T = 5.0$, $\xi = 2z_0/7$, $\eta_{\rm s} = \eta_{\rm b} = 0.1$ are set. Comparison between Figs. 9(a) and 9(b) suggests that the species separation is enhanced as the size ratio is increased. Most of the big particles are expelled towards the confining walls because of the stronger depletion in the vicinity of the walls. From the point view of AO, the larger size ratio, the larger area where the small particle is inaccessible when two big particles is approaching. The enhanced depletion may cause more significant separation in mixture. In addition, as shown in the inset of Fig. 9(b), few big particle is observed in the middle region of the pore. This is again the result of the competition between the depletion and the external potential. The relatively dominant depletion leads to the survival of the big particles there.

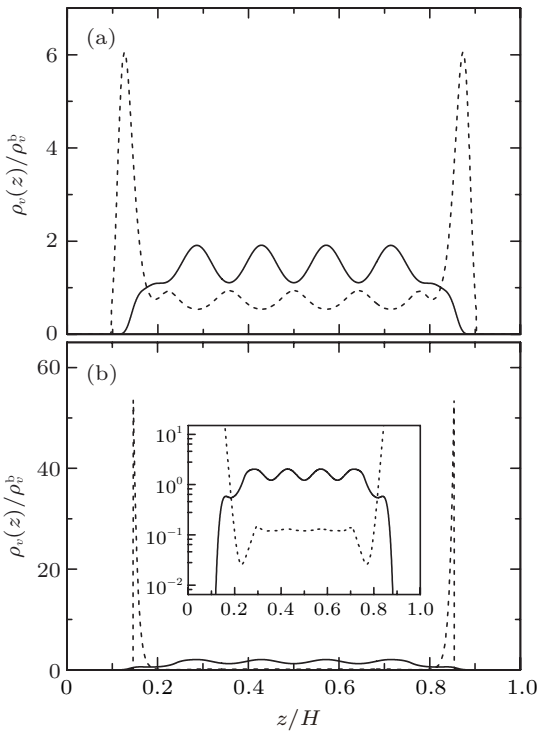


Fig. 9. Equilibrium density profiles of the binary mixture along the z direction under different conditions of size ratios. Panels (a) and (b) correspond respectively to $\sigma_{\rm b}/\sigma_{\rm s} = 2.0$ and 3.0. The solid and dash lines correspond respectively to the small and big species. The inset in panel (b) shows the detail of the equilibrium density profiles in the middle region of the pore.

4. Conclusion

Based on classical DFT for the binary mixture, the species separation of binary colloidal mixture confined between two walls is investigated. In this work, the mixture is subject to an external multi-Gauss potential, which is composed of seven Gauss barriers. The density of both species is calculated when the geometry of the multi-Gauss trap is adjusted. The numerical results suggest that the barrier width, barrier distance, barrier height, and size ratio influence the species separation and phase equilibrium in different ways.

For the given barrier height and distance, the strong external force induced by the narrow and sharp barrier leads to the disappearance of both species at the position where the barrier locates. With the increase of barrier width, depletion potential takes more advantage, which is responsible for the species separation of the mixture. For the given barrier width and height, the barrier distance determines the coupling between barriers, which will in turn influence the depletion potential. As the barriers are very close to each other, it can be regarded as one new barrier with a larger height. For the given barrier width and distance, the height plays an important role in the competition between the external potential and the depletion potential. Usually, the larger the barrier height, the stronger the depletion is. However, when the barrier height is extremely large, the external potential is dominant in its competition with the depletion, which leads to the disappearance of both species there.

In conclusion, the competition between the external potential and the depletion potential is the deciding factor in the species separation of asymmetrical colloidal mixture. It is hoped that the results and analysis in this work may provide useful clues to understand the species separation of colloidal system. Recently, Niu *et al.*[48] theoretically studied the symmetrical adhesion of two cylindrical colloids to a tubular membrane with the full treatment of the Helfrich model. By analyzing the energy of the system, a second-order adhesion transition and a first-order phase transition were obtained. It is expected that our results in this work can be useful for understanding these complex colloidal systems and their phenomena behavior.

Acknowledgments

The author Sun Zong-Li would like to acknowledge Anil Kumar A V for his useful suggestions and his generosity to send the simulation data.

References

[1] Asakura S and Oosawa F 1954 *J. Chem. Phys.* **22** 1255
[2] Vrij A 1976 *Pure Appl. Chem.* **48** 471
[3] Nonner W, Catacuzzeno L and Eisenberg R S 2000 *Biophys. J.* **79** 1976
[4] Hille B 2001 *Ion Channels of Excitable Membranes* (Sunderland: Sinauer Asc.)

[5] Gillespie D, Nonner W, Henderson D and Eisenberg R S 2002 *Phys. Chem. Chem. Phys.* **4** 4763
[6] Roth R and Gillespie D 2005 *Phys. Rev. Lett.* **95** 247801
[7] Ye X, Narayanan T, Tong P, Huang J S, Lin M Y, Carvalho B L and Fetters L J 1996 *Phys. Rev. E* **54** 6500
[8] Brader J M, Dijkstra M and Evans R 2001 *Phys. Rev. E* **63** 041405
[9] Louis A A, Bolhuis P G, Meijer E J and Hansen J P 2002 *J. Chem. Phys.* **117** 1893
[10] Tuinier R, Rieger J and de Kruif C G 2003 *Adv. Col. Int. Sci.* **103** 1
[11] Chen X, Cai J, Liu H and Hu Y 2006 *Mol. Sim.* **32** 877
[12] Li Z D and Wu J Z 2007 *J. Chem. Phys.* **126** 144904
[13] Bryant G, Williams S R, Qian L, Snook I K, Perez E and Pincet F 2002 *Phys. Rev. E* **66** 060501
[14] You F Q, Yu Y X and Gao G H 2005 *J. Phys. Chem. B* **109** 3512
[15] Yu Y X, You F Q, Tang Y P, Gao G H and Li Y G 2006 *J. Phys. Chem. B* **110** 334
[16] Yu Y X and Jin L 2008 *J. Chem. Phys.* **128** 014901
[17] Roth R, Evans R and Dietrich S 2000 *Phys. Rev. E* **62** 5360
[18] Ashton D J, Wilding N B, Roth R and Evans R 2011 *Phys. Rev. E* **84** 061136
[19] Roth R, Rauscher M and Archer A J 2009 *Phys. Rev. E* **80** 021409
[20] Anil Kumar A V 2013 *J. Chem. Phys.* **138** 154903
[21] Lekkerkerker H N W and Stroobats A 1993 *Physica A* **195** 387
[22] Mao Y, Cates M E and Lekkerkerker H N W 1995 *Physica A* **222** 10
[23] Götzelmann B, Evans R and Dietrich S 1998 *Phys. Rev. E* **57** 6785
[24] Götzelmann B, Roth R, Dietrich S, Dijkstra M and Evans R 1999 *Europhys. Lett.* **47** 398
[25] Roth R, Evans R and Dietrich S 2000 *Phys. Rev. E* **62** 5360
[26] Méndez-Alcaraz J M and Klein R 2000 *Phys. Rev. E* **61** 4095
[27] Castañeda-Priego R, Rodríguez-López A and Méndez-Alcaraz J M 2003 *J. Phys.: Condens. Matter* **15** S3393
[28] González-Mozuelos P, Méndez-Alcaraz J M and Castañeda-Priego R 2005 *J. Chem. Phys.* **123** 214907
[29] Castañeda-Priego R, Rodríguez-López A and Méndez-Alcaraz J M 2006 *Phys. Rev. E* **73** 051404
[30] Evans R 1979 *Adv. Phys.* **28** 143
[31] Henderson D 1992 *Fundamentals of Inhomogeneous Fluids* (New York: Dekker)
[32] Hansen J P and McDonald I R 1986 *Theory of Simple Liquids*, 2nd edn. (New York: Academic Press)
[33] Sun Z L, Kang Y S, Kang Y M, Liu Z C and Ma H X 2012 *Chin. Phys. B* **21** 066103
[34] Yu Y X 2009 *J. Chem. Phys.* **131** 024704
[35] Ramakrishnan T V and Yussouff M 1979 *Phys. Rev. B* **19** 2775
[36] Calleja M, North A N, Powels J G and Rickayzen G 1991 *Mol. Phys.* **73** 973
[37] Zhou S Q and Ruckenstein E 2000 *Phys. Rev. E* **61** 2704
[38] Zhou S Q and Ruckenstein E 2000 *J. Chem. Phys.* **112** 8079
[39] Choudhury N and Ghosh S K 2001 *J. Chem. Phys.* **114** 8530
[40] Kim S C and Suh S Y 2002 *J. Chem. Phys.* **117** 9880
[41] Tarazona P 1985 *Phys. Rev. A* **31** 2672
[42] Curtin W A and Ashcroft N W 1985 *Phys. Rev. A* **32** 2909
[43] Rosenfeld Y 1989 *Phys. Rev. Lett.* **63** 980
[44] Roth R, Evans R, Lang A and Kahl G 2002 *J. Phys.: Condens. Matter* **14** 12063
[45] Yu Y X and Wu J Z 2002 *J. Chem. Phys.* **117** 10156
[46] Yu Y X, Wu J Z, Xin Y X and Gao G H 2004 *J. Chem. Phys.* **121** 1535
[47] You F Q, Yu Y X and Gao G H 2005 *J. Chem. Phys.* **123** 114705
[48] Niu Y Q, Wei W, Zheng B, Zhang C X and Meng Q T 2013 *Chin. Phys. B* **22** 128701